RSC Advances

ROYAL SOCIETY OF CHEMISTRY

www.rsc.org/advances

RSC Advances

COMMUNICATION

Enhanced photocatalysis activity of ferroelectric $KNbO_3$ nanofibers compared with anti-ferroelectric $NaNbO_3$ nanofibers synthesized by electrospinning

Received 00th January 20xx,
Accepted 00th January 20xx

DOI: 10.1039/x0xx00000x

www.rsc.org/

Yu Huan,[a] Xiaohui Wang,[a] Weichang Hao[c] and Longtu Li[a]

Perovskite-type alkalis niobate nanofibers were prepared by electrospinning. $KNbO_3$ nanofibers with lower BET perform higher photocatalytic efficiency than $NaNbO_3$ with similar phase structure and morphology. The internal electric field, which does not exist in anti-ferroelectric $NaNbO_3$, induced by spontaneous polarization in ferroelectric $KNbO_3$ can promote separation and accelerate movement of photo-generated charge carries.

Introduction

Since TiO_2 was firstly reported by Honda *et al.*[1] to have photocatalytic activity in hydrogen evolution, semiconductor photocatalysis have been found to have important applications in clean hydrogen energy generation and organic pollutant treatments. The study of novel semiconductor photocatalysts, such as Ti-, Nb-, and Ta-based photocatalysts, is an important issue during the past decades.[2-4] Among these materials, perovskite-type oxides are attractive because of their high stability, good availability and low toxicity under light illumination. It is well known that the efficiency of photocatalysts is determined by not only its band gap but also the ability to separate photo-generated charge carries. The ferroelectric material exhibits considerable photocatalytic performance because the existence of the internal electric field constructed by the spontaneous polarization. The internal electric field can effectively promote the separation of the electrons and holes and accelerate the movement of electrons and holes in opposite directions.[5] Thus, the ferroelectric materials such as PSZT[6] and $BiFeO_3$[7] have attracted a lot of attention in the decade years. However, these materials fatally contain large quantities of the toxic element Pb and Bi. Environmentally friendly $ANbO_3$ (A = K, Na) has attracted substantial interest among researchers and equipment designers because of its unique physical properties.[8, 9] Although a few studies focused on the photocatalytic activity of $ANbO_3$ powders,[10-13] they do not shed any light on the correlation between the enhanced photocatalytic activity and the internal electric field in the ferroelectric material.

In view of scientific interest and potential commercial applications, the photocatalytic activities of the previously reported $ANbO_3$ micro-powders are still not high enough because of the low Brunauer-Emmett-Teller (BET) surfaces.[10-12] Recently, one-dimensional (1D) nanostructures are expected to result in much higher photocatalytic activities for the large surface-volume ratio and high surface activity.[14, 15] Compared to hydrothermal method[16] and molten salt method[17], electrospinning is the simplest and most versatile technique capable of generating nanofibers. Meanwhile the electrospun nanofibers have high aspect ratio, controllable fiber diameters and precise chemical stoichiometric composition.[18]

In this study, $ANbO_3$ nanofibers were prepared by sol-gel based electrospinning. We apply $ANbO_3$ nanofibers in the degradation for rhodamine B (RhB) which is a preventative dye pollutant in photocatalytic activity determination. To our best of knowledge, this study is the first report on $ANbO_3$ electrospun nanofibers in photocatalysis. Our experimental results indicate the higher photocatalytic activity could be obtained in the ferroelectric $KNbO_3$ nanofibers compared with anti-ferroelectric $NaNbO_3$ nanofibers because of the internal polar field induced by spontaneous polarization. The synthesis and characterization of $KNbO_3$ and $NaNbO_3$ nanofibers are shown in the supporting information.

Results and Discussion

The $KNbO_3$ and $NaNbO_3$ binder-contained fibers after drying at 80 °C for 5 h in a vacuum oven are abbreviate to be KN-NF and NN-NF, respectively. Figure 1b displays the Fourier transform infrared spectroscopy (FTIR) spectra of the $KNbO_3$ samples and raw materials. The characteristic band at ca. 1620 cm^{-1} corresponds to the C=O stretching vibration of acetylacetone. 2-methoxyethanol shows two C–O stretching modes, one at ca. 1124 cm^{-1} characteristic of an ether with $–CH_2–O–CH_2–$ grouping and another at ca. 1066 cm^{-1}, which is characteristic of a primary alcohol.[19] It is

[a] State Key Laboratory of New Ceramics and Fine Processing, School of Materials Science and Engineering, Tsinghua University, Beijing 100084, China.
[b] Department of Physics, and Key Laboratory of Micro-nano Measurement, Manipulation and Physics, Ministry of Education (MOE), Beihang University, Beijing 100191, China.
† Author to whom correspondence should be addressed; Email: wxh@mail.tsinghua.edu.cn.
Electronic Supplementary Information (ESI) available: [details of any supplementary information available should be included here]. See DOI: 10.1039/x0xx00000x

hard to detect the three peaks in the FTIR spectra of KN-NF and NN-NF, illustrating that the solvent volatilizes completely. The double bands at ca. 1105 and 1066 cm^{-1} of niobium ethoxide do not appear in the spectra of KN-NF and NN-NF, demonstrating that niobium ethoxide is decomposed to niobium hydroxide. The bands at ca. 1574 and 1425 cm^{-1} are assignable to stretching vibration and antisymmetric stretching vibration of carboxyl, respectively, which appear in the FTIR spectra of KN-NF and NN-NF demonstrating that the alkalis acetates exist in KN-NF and NN-NF.

KN-NF was calcined at 500 °C, 600 °C, 700 °C, 800 °C in air, which are abbreviated to be KN-NF-500, KN-NF-600, KN-NF-700, KN-NF-800, respectively. For the KN-NF of thermogravimetric-differential scanning calorimetry (TG-DSC) curves as shown in Fig. 1a, the endothermic peak at 130 °C in the DSC curve should attribute to the decomposition of CH_3COOK. Subsequently, about 30% weigh loss is observed at 280 °C in the TG curve accompanied by the corresponding endothermic peak in the DSC curve, resulting from the combustion of PVP. The weak endothermic peak at ca. 400 °C should be assigned to the elimination of crystallization water in niobium hydroxide because part of crystallization water is difficult to be eliminated until 400 °C. The endothermic peak at ca. 580 °C should be ascribed to the crystallization of $KNbO_3$. There are some peaks in FTIR spectrum of the KN-NF-500, which should be ascribed to the peaks of the resident organism. All the characteristic peaks corresponding to the organic functional groups in the FTIR spectrum have disappeared in KN-NF-600. The band around 500 cm^{-1} can be assigned to the edge-shared NbO_6 octahedron and the broad, strong band centered at *ca.* 623 cm^{-1} represents the O–Nb–O stretching vibration in the corner-shared NbO_6[12], demonstrating that perovskite structure forms when the KN-NF is calcined above 600 °C in agreement with X-Ray diffraction (XRD) profiles in Fig. 1b. The $KNbO_3$ could be well indexed to the orthorhombic phase with JCPDS No. 71-0946 without the second phase. The endothermic peak at ca. 670 °C should be ascribed to the grain growth of $KNbO_3$ because no significant change appears in FTIR and XRD spectra. Because the crystallinity of KN-NF-600 is low from the Raman spectra (Fig. S1a), the calcination temperature is designated to 700 °C. The weak endothermic peak at ca. 860 °C should attribute to the fracture of the nanofibers.

The TG-DSC curve of NN-NF shows similar features with that of KN-NF except for a few differences. Firstly, the combustion of PVP occurs from ca. 200 to 380 °C accompanied by the endothermic peak in the DSC curve. Secondly, the decomposition of CH_3COONa is indexed the endothermic peak at ca. 390 °C in the DSC curve because CH_3COONa decomposes at higher temperature than CH_3COOK. Thirdly, the crystallization of $NaNbO_3$ should happen at ca. 580 °C accompanied by the corresponding endothermic peak. To determine the calcination temperature, the NN-NF are calcined at 400 °C, 500 °C, 600 °C, 700 °C in air, which are abbreviate to be NN-NF-400, NN-NF-500, NN-NF-600, NN-NF-700, respectively. From the FTIR spectra in Fig. 1e, the bands of organic functional groups do not disappear until calcining at 500 °C. There are two different phases of $NaNbO_3$, anti-ferroelectric (*Pbma*, JCPDS No. 89-8957) and ferroelectric (*$P2_1ma$*, JCPDS No. 82-0606).[20] The XRD pattern of NN-NF calcined above 500 °C could be well indexed to the space group *Pbma* as displayed in Fig. 1f, demonstrating the $NaNbO_3$ nanofibers show anti-ferroelectric properties. The characteristic peaks of NbO_6 octahedra distinctly appear when the NN-NF calcined at 600 °C from the Raman spectra (Fig. S1b). Therefore, the best calcination temperature for treatment of NN-NF is 600 °C.

From the scanning electron microscope (SEM) in Fig. 2a1 and 2b1, KN-NF and NN-NF have a relatively uniform diameter of ca. 500 nm. After calcining, the surface of the nanofibers is not quite smooth because of grain growth at high temperature, as shown in Fig. 2a2 and 2b2. Those nanofibers compactly stack together by small nanoparticles from the transmission electron microscopy (TEM) bright images as shown in Figs. 2a3 and 2b3. The nanofibers are polycrystalline from the selected area electron diffraction (SAED) with several sets of spot patterns obtained from part nanofibers as shown in insets of Fig. 2a3 and 2b3. Meanwhile, the regular atomic arrangement, as depicted in high resolution transmission electron microscopy (HRTEM) images of Fig. 2a4 and 2b4, indicates that the synthesized nanofibers have good crystallinity. The crystal lattice spacing of 0.406 nm and 0.285 nm correspond to (011) and (200) crystal planes of orthorhombic $KNbO_3$, respectively, which agrees well with the results obtained from the SAED pattern in inset. The angle of adjacent spots labeled in the SAED pattern is 90°, which is identical to the theoretical value of the angle between the (011) and (200) planes of orthorhombic $KNbO_3$. Analogously, the crystal lattice spacing of 0.391 nm and 0.389 nm in NN-NF-600 is well ascribed to (101) and (040) crystal planes of the orthorhombic $NaNbO_3$, respectively. In order to clarify the grain size of nanofibers, dark-field TEM (DFTEM) images are illustrated in Fig. 2. The DFTEM images in Fig. 2a5 and 2a6 are obtained using the A and B reflections in inset of Fig. 2a3, respectively. Typically, the nanofibers are stacked one by one by small nanoparticles together with the grain size of about 200 nm. Similar conclusions apply to the NN-NF-600. Furthermore, energy-dispersive X-ray spectroscopy (EDS) mapping indicate that all the chemical elements distribute homogeneously as shown in Fig. S2.

The photocatalytic activity of as-prepared samples was evaluated using RhB aqueous solution degradation under UV-Vis light illumination. The change of relative RhB aqueous solution concentration as a function of irradiation time (*t*) is shown in Fig. 3a. For the blank experiment, RhB aqueous solution degradation under UV-Vis light illumination is negligible. The RhB aqueous solution concentration decreases with the increase of reaction time, demonstrating the RhB molecule is decomposed. The decomposition rate declines because the RhB aqueous solution concentration decreases. To evaluate the photoreactivity quantitatively, the reaction rate constants are calculated and depicted in Fig. 3b. The photodegradation of RhB in the present of $KNbO_3$ and $NaNbO_3$ can be considered as a pseudo-first-order reaction[13], and its kinetics can be expressed as follows:

$$C = C_0 e^{-kt}$$

where *k* is the degradation rate constant, and C_0 and *C* are the initial concentrations of RhB and that under *t*, respectively. Fig. 3b shows the relationship between $\ln(C_0/C)$ and *t* with the corresponding fitting curves. It is found that the degradation rate constants with the KN-NF-700 and NN-NF-600 are 0.01281 min^{-1}, 0.00982 min^{-1}, respectively, though NN-NF-600 owns larger BET specific surface area as shown in Table 1. When divide the reaction rate constant by the BET specific surface area, the KN-NF-700 exhibits better photocatalytic activity than NN-NF-600 as shown in

the right graph of Fig. 3c. It is well known that the efficiency of photocatalyst is determined mainly by its band gap energy (E_g) and ability to separate photogenerated charge carries (electrons and holes). E_g is estimated by UV-Vis diffusion reflectance spectra in Fig. 3d. Extend the linear part of the spectral line as the black dotted line in Fig. 3d and find the intersection of the black dotted line and x-axis. Divide 1240 by wavelength of the intersection, and we can estimate E_g. It is obvious that E_g of the NN-NF-600 are slightly larger than that of KN-NF-700 as shown in Table 1, resulting in the low effective utilization of irradiations of NN-NF-600. Moreover, $KNbO_3$ with orthorhombic phase is ferroelectric while $NaNbO_3$ with orthorhombic phase is anti-ferroelectric. To prove the ferroelectric properties of the nanoscale KN-NF-700 prepared in this study, the effective piezoelectric coefficient d_{33}^* was measured by a modified atomic force microscopy (AFM) system. The Si cantilever tip is Pt-coated and conductive. KN-NF-700 was dropped on the Pt-coated silicon ($Pt/Ti/SiO_2/Si$) substrates after being ultrasonic dispersed in ethanol. An individual KN-NF-700 nanofiber was detected by AFM in the experiment as shown in Fig. 4a. Then keep the cantilever tip fixed above the interesting point of the nanofiber, and apply an alternating current voltage from -9 to 9 V while recording the piezoelectric displacement by laser, the result of the measurement of d_{33}^* is shown in Fig. 4b. The individual nanofiber presented piezoelectric property, as typical well-shaped displacement-voltage "butterfly" loop, indicating that $KNbO_3$ nanofibers is ferroelectric material though the grain size is very small. As the schematic diagram in Fig. 5, the domain exists in the $KNbO_3$ grains and the internal electric field is induced by the spontaneous polarization. When the ferroelectric photocatalyst is illuminated by UV-Vis light with photon energy higher than E_g, electrons in the valence band can be excited to the conduction band with simultaneous generation of the same amount of holes left behind. The internal electric field in $KNbO_3$ nanofibers promotes the separation of the electrons and holes and accelerates electrons and holes to move spatial in opposite directions. These phenomena are analogous to the behavior of charge carriers under an external electric fields. Bastard *et al.*[21] reported that the conduction band and valence band electrons in GaAs quantum wells can be spatially separated by applying an external electric field. However, there is no internal electric field because the $NaNbO_3$ is anti-ferroelectrics. The photo-generated electrons and holes will more easily recombine before they migrate to the surface leading to the depressed photocatalytic activity. Thus, it is reasonable to suppose that photo-generated electron-hole pairs of the ferroelectric materials can be effectively separated by the internal polar field caused by spontaneous polarization and hence enhance photocatalytic activity. In addition, the XRD and XPS patterns of the samples after photocatalytic reactions are the nearly same as those of the fresh photocatalyst (Figs. S4 and S5), indicating the high stability against chemical reaction during photocatalytic reaction. The KN-NF-700 and NN-NF-600 can be recycled by filtration. Thus, the $KNbO_3$ and $NaNbO_3$ nanofibers may be the attractive candidates as photocatalysts.

Conclusion

The $KNbO_3$ and $NaNbO_3$ nanofibers with uniform diameter of ca. 500 nm were prepared by sol-gel based electrospinning. The perovskite-type $KNbO_3$ and $NaNbO_3$ nanofibers were well crystallized after being calcined at 700 and 600 °C, respectively. The nanofibers are composed of small nanoparticles compactly stacked one by one revealed by DFTEM analysis. The ferroelectric $KNbO_3$ nanofibers, whose ferroelectric properties is proved by the modified AFM, with lower BET surface areas shows higher photocatalytic activity than the anti-ferroelectric $NaNbO_3$ nanofibers with the similar phase structure and micromorphology. It is found that the spontaneous polarization in the ferroelectric domain can induce the internal polar electric field, which can promote the separation of the photo-generated electrons and holes and accelerate the movement of electrons and holes in opposite directions. In addition, the $KNbO_3$ and $NaNbO_3$ nanofibers with good availability and low toxicity show the high stability under irradiation. Therefore, it is potentially to develop nanoscale multifunctional devices because $KNbO_3$ has the applications in actuators, sensors, transducer, and capacitor.

Acknowledgements

The work was supported by Ministry of Sciences and Technology of China through National Basic Research Program of China (973 Program 2015CB654604), National Natural Science Foundation of China for Creative Research Groups (Grant No.51221291), National Natural Science Foundation of China (Grant Nos. 51272123, 51332002), and also supported by CBMI Construction Co., Ltd. W. Hao thanks National Natural Science Foundation of China for partial support of this work (Grant Nos. 51272015, 51472016).

References

1. A. Fujishima and K. Honda, *Nature*, 1972, **238**, 37-38.
2. M. R. Hoffmann, S. T. Martin, W. Y. Choi and D. W. Bahnemann, *Chem. Rev.*, 1995, **95**, 69-96.
3. Q. J. Xiang, J. G. Yu and M. Jaroniec, *Chem. Soc. Rev.*, 2012, **41**, 782-796.
4. Y. Inoue, *Energy Environ. Sci.*, 2009, **2**, 364-386.
5. J. Jiang, K. Zhao, X. Xiao and L. Zhang, *J. Am. Chem. Soc.*, 2012, **134**, 4473-4476.
6. Y. Inoue, K. Sato and K. Sato, *J. Chem. Soc., Faraday Trans 1*, 1989, **85**, 1765-1774.
7. F. Gao, Y. Yuan, K. Wang, X. Chen, F. Chen, J.-M. Liu and Z. Ren, *Appl. Phys. Lett.*, 2006, **89**, 102506.
8. P. Günter, *Phys. Rep.*, 1982, **93**, 199-299.
9. J. Richter, A. Steinbrück, M. Zilk, A. Sergeyev, T. Pertsch, A. Tünnermann and R. Grange, *Nanoscale*, 2014, **6**, 5200-5207.
10. G. Q. Li, T. Kako, D. F. Wang, Z. G. Zou and J. H. Ye, *J. Phys. Chem. Solids*, 2008, **69**, 2487-2491.
11. L. S. Yan, J. Zhang, X. M. Zhou, X. X. Wu, J. Y. Lan, Y. S. Wang, G. Liu, J. G. Yu and L. J. Zhi, *Int. J. Hydrogen Energy*, 2013, **38**, 3554-3561.
12. T. T. Zhang, K. Zhao, J. G. Yu, J. Jin, Y. Qi, H. Q. Li, X. J. Hou and G. Liu, *Nanoscale*, 2013, **5**, 8375-8383.
13. J. Y. Lan, X. Zhou, G. Liu, J. G. Yu, J. C. Zhang, L. J. Zhi and G. J. Nie, *Nanoscale*, 2011, **3**, 5161-5167.
14. Y. Wang, X. Zhan, F. Wang, Q. Wang, M. Safdar and J. He, *J. Mater. Chem. A*, 2014, **2**, 18413-18419.
15. N. C. Hildebrandt, J. Soldat and R. Marschall, *Small*, 2015, **11**, 2051-2057.
16. Y. Xu, Q. Yu and J. F. Li, *J. Mater. Chem.*, 2012, **22**, 23221-23226.

17. L. Li, J. Deng, J. Chen, X. Sun, R. Yu, G. Liu and X. Xing, *Chem. Mater.*, 2009, **21**, 1207-1213.
18. X. F. Lu, C. Wang and Y. Wei, *Small*, 2009, **5**, 2349-2370.
19. C. Guha, J. M. Chakraborty, S. Karanjai and B. Das, *J. Phys. Chem. B*, 2003, **107**, 12814-12819.
20. T. Y. Ke, H. A. Chen, H. S. Sheu, J. W. Yeh, H. N. Lin, C. Y. Lee and H. T. Chiu, *J. Phys. Chem. C*, 2008, **112**, 8827-8831.
21. G. Bastard, E. Mendez, L. Chang and L. Esaki, *Phys. Rev. B*, 1983, **28**, 3241.

Figure captions:

Figure 1 (a) TG-DSC curves of KN-NF, (b) FTIR spectra of the raw materials and the KN-NF calcined at different temperatures, (c) XRD patterns of KN-NF calcined at different temperatures, (d) TG-DSC curves of NN-NF, (e) FTIR spectra of the raw materials and the NN-NF calcined at different temperatures, (f) XRD patterns of NN-NF calcined at different temperatures

Figure 2 SEM images of (a1) KN-NF; (a2) KN-NF-700; (a3) TEM image of KN-NF-700, inset: the corresponding SAED pattern; (a4) HRTEM image of KN-NF-700, inset: the corresponding SAED pattern; (a5, a6) DFTEM images taken using the A and B reflections in figure a3. (b1) NN-NF; (b2) NN-NF-600; (b3) TEM image of NN-NF-600, inset: the corresponding SAED pattern; (b4) HRTEM image of NN-NF-600, inset: the corresponding SAED pattern; (b5, b6) DFTEM images taken using the C and D reflections in figure b3.

Figure 3 (a) photodegradation curves of RhB aqueous solution with photocatalyst, (b) linear least-squares fitting of $\ln(C/C_0)$ versus irradiation time plots, (c) reaction rate constant and reaction rate constant per unit area of the photocatalyst, (d) UV-Vis diffusion reflectance spectra of KN-NF-700 and NN-NF-600

Figure 4 (a) Top view of an individual $KNbO_3$ nanofiber, (b) Displacement-Voltage curve (black line) and d_{33}-Voltage curve (red line)

Figure 5 Schematic diagram of the domain structure and spontaneous polarization direction in unit cell in (a) KN-NN-700 and (b) NN-NF-600

Table 1 BET surface areas and band gap of the as-prepared samples

Samples	BET surface areas (m^2/g)	Band Gap (eV)
KN-NF-700	10.098	3.626
NN-NF-600	15.668	3.804

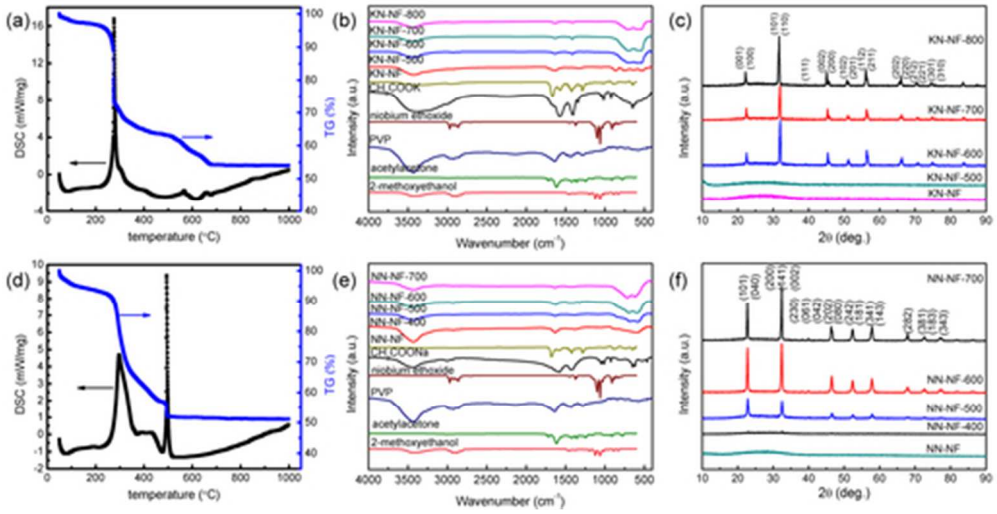

Figure 1 (a) TG-DSC curves of KN-NF, (b) FTIR spectra of the raw materials and the KN-NF calcined at different temperatures, (c) XRD patterns of KN-NF calcined at different temperatures, (d) TG-DSC curves of NN-NF, (e) FTIR spectra of the raw materials and the NN-NF calcined at different temperatures, (f) XRD patterns of NN-NF calcined at different temperatures
43x22mm (300 x 300 DPI)

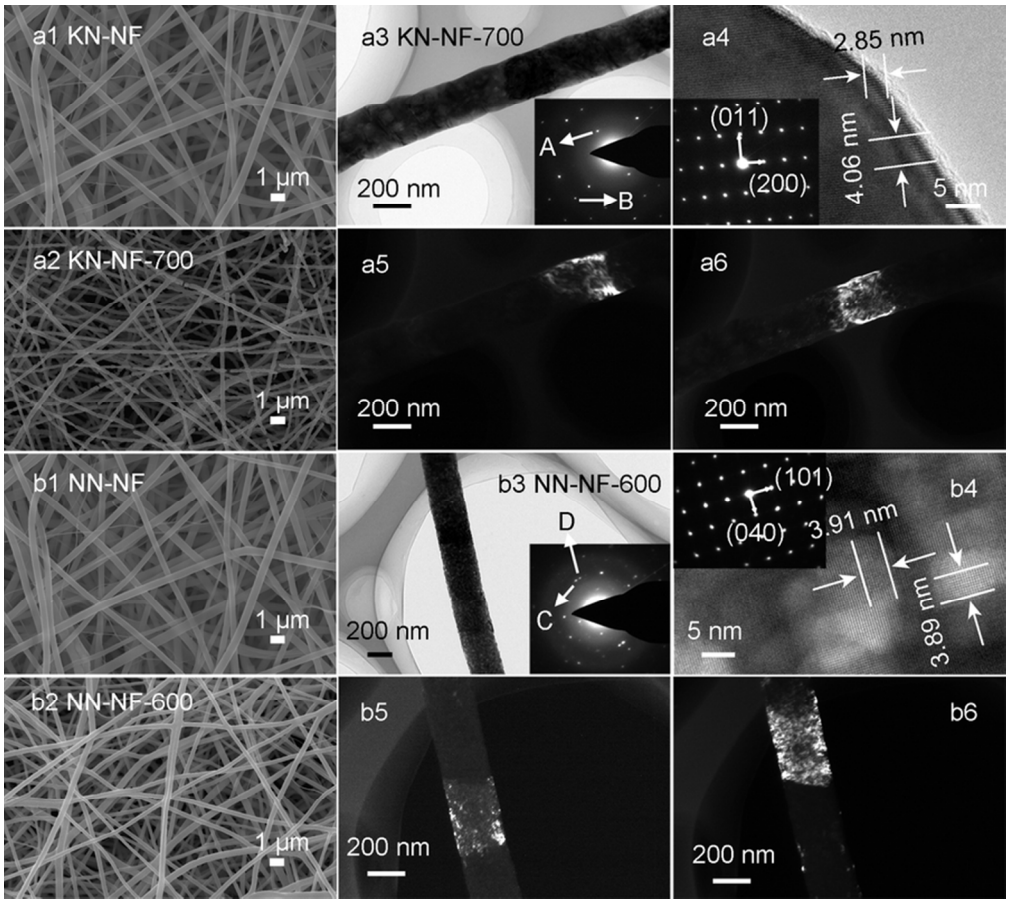

Figure 2 SEM images of (a1) KN-NF; (a2) KN-NF-700; (a3) TEM image of KN-NF-700, inset: the corresponding SAED pattern; (a4) HRTEM image of KN-NF-700, inset: the corresponding SAED pattern; (a5, a6) DFTEM images taken using the A and B reflections in figure a3. (b1) NN-NF; (b2) NN-NF-600; (b3) TEM image of NN-NF-600, inset: the corresponding SAED pattern; (b4) HRTEM image of NN-NF-600, inset: the corresponding SAED pattern; (b5, b6) DFTEM images taken using the C and D reflections in figure b3.
75x67mm (300 x 300 DPI)

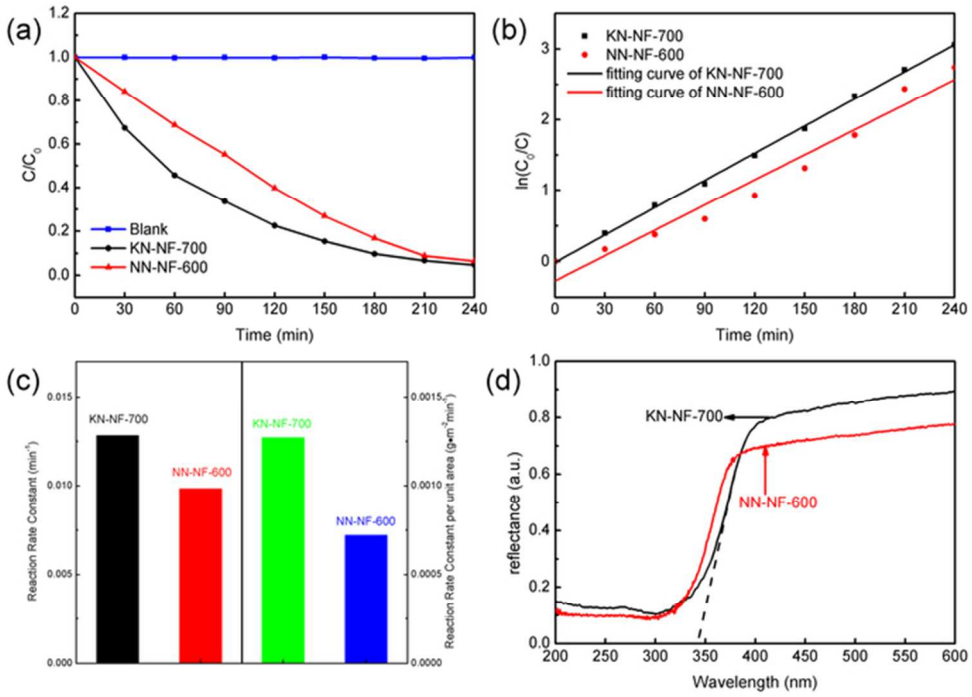

Figure 3 (a) photodegradation curves of RhB aqueous solution with photocatalyst, (b) linear least-squares fitting of ln(C/C0) versus irradiation time plots, (c) reaction rate constant and reaction rate constant per unit area of the photocatalyst, (d) UV-Vis diffusion reflectance spectra of KN-NF-700 and NN-NF-600
59x42mm (300 x 300 DPI)

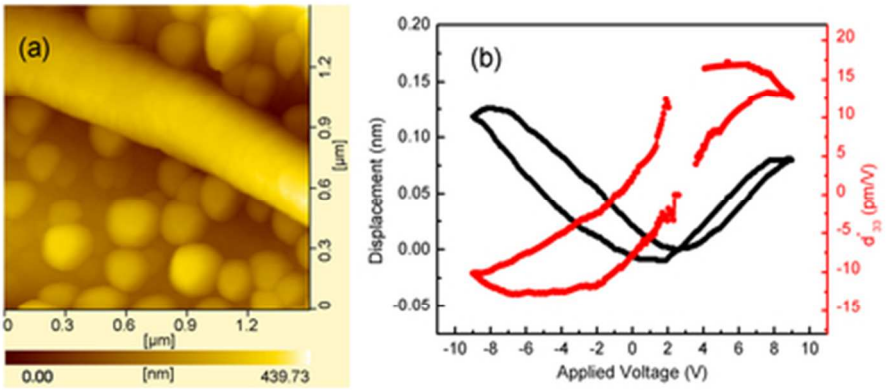

Figure 4 (a) Top view of an individual KNbO3 nanofiber, (b) Displacement-Voltage curve (black line) and d33-Voltage curve (red line)
38x17mm (300 x 300 DPI)

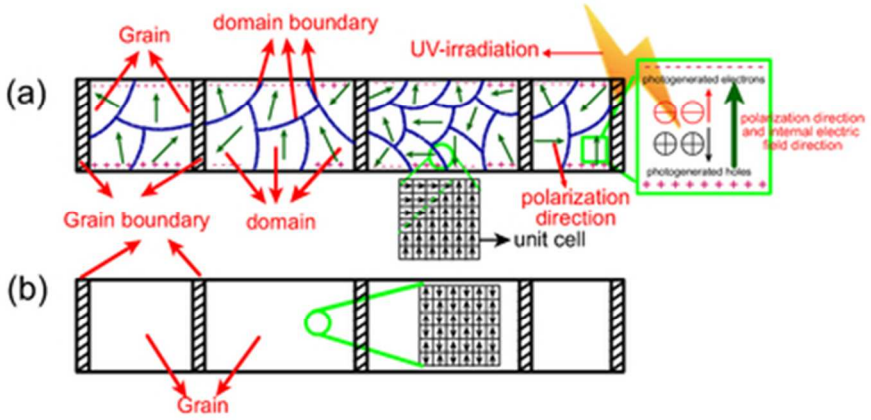

Figure 5 Schematic diagram of the domain structure and spontaneous polarization direction in unit cell in (a) KN-NN-700 and (b) NN-NF-600
39x18mm (300 x 300 DPI)